A search for photometric variability towards M71 with the Near-Infrared Transiting ExoplanetS Telescope

J. McCormac,[1,2]★ I. Skillen,[1] D. Pollacco,[2,3] F. Faedi,[2,3] G. Ramsay,[4] V. S. Dhillon,[5] I. Todd[2] and A. Gonzalez[1,6]

[1]*Isaac Newton Group of Telescopes, Apartado de Correos 321, E-38700, Santa Cruz de la Palma, Spain*
[2]*Astrophysics Research Centre, School of Mathematics and Physics, Queen's University, Belfast BT7 1NN, UK*
[3]*Department of Physics, University of Warwick, Coventry CV4 7AL, UK*
[4]*Armagh Observatory, College Hill, Armagh BT61 9DG, UK*
[5]*Department of Physics and Astronomy, University of Sheffield, Sheffield S3 7RH, UK*
[6]*Instituto de Astrofísica de Canarias, E-38205 La Laguna, Spain*

ABSTRACT

We present the results of a high-cadence photometric survey of an 11 arcmin × 11 arcmin field centred on the globular cluster M71, with the Near-Infrared Transiting ExoplanetS Telescope. The aim of our survey is to search for stellar variability and giant transiting exoplanets. This survey differs from previous photometric surveys of M71 in that it is more sensitive to lower amplitude ($\Delta M \leq 0.02$ mag) and longer period ($P > 2$ d) variability than previous work on this cluster. We have discovered 17 new variable stars towards M71 and confirm the nature of 13 previously known objects, for which the orbital periods of 7 are refined or newly determined. Given the photometric precision of our high-cadence survey on the horizontal branch of M71, we confirm that the cluster is devoid of RR Lyrae variable stars within the area surveyed. We present new B- and V-band photometry of the stars in our sample from which we estimate spectral types of the variable objects. We also search our survey data for transiting hot Jupiters and present simulations of the expected number of detections. Approximately 1000 stars were observed on the main sequence of M71 with sufficient photometric accuracy to detect a transiting hot Jupiter; however, none were found.

Key words: instrumentation: photometers – techniques: photometric – planetary systems – stars: variables: general – globular clusters: individual: M71 – globular clusters: individual: NGC 6838.

1 INTRODUCTION

M71 (NGC 6838) is a sparsely populated, metal-rich globular cluster (GC), located at RA (J2000) $19^h\,53^m\,46\overset{s}{.}49$, Dec. (J2000) $+18°\,46'\,45\overset{''}{.}1$, at a distance of 3.6 kpc from the Sun (Geffert & Maintz 2000, hereafter GM00), in a crowded field not far from the Galactic plane, $l = 56\overset{\circ}{.}7$ and $b = -4\overset{\circ}{.}6$ (Golsbury et al. 2000). The earliest modern work on variable stars in M71 was carried out by Sawyer (1953), who discovered four bright variables in the region towards the cluster, one of which is the long-period semi-regular pulsating giant Z Sagittae and another the semi-detached Algol-type eclipsing binary QU Sge.

The first systematic photometric study of M71 was conducted by Arp & Hartwick (1971, hereafter AH71) with the goal of determining the age of the cluster and creating an accurate colour–magnitude diagram (CMD). AH71 carried out *UBV* photographic and photo-electric observations of M71, calculating the reddening, distance modulus and age of the system to be $E(B - V) = 0.31 \pm 0.02$, $(m - M)_0 = 13.07 \pm 0.21$ and age $= 7.6^{+3.1}_{-2.3}$ Gyr, respectively. Cudworth (1985) conducted a cluster membership survey of over 350 stars towards M71 with $V < 16$ using proper motions.

In the early 1990s, two photometric surveys were carried out in the central region of M71 by Hodder et al. (1992) and Yan & Mateo (1994), discovering four and five new variable stars, respectively. Hodder et al. (1992) concluded that one of the 10 blue stragglers observed is a variable star (H1) of the SX Phoenicis (SX Phe) type. The second variable (H2) is possibly a field dwarf Cepheid (δ Scuti) and the remaining two variables (H3 and H4) are possible eclipsing binaries. The goal of the survey by Yan & Mateo (1994) was to determine the primordial binary percentage in M71. Three of the variables they discovered are contact binaries (V1, V2 and V5), while the remaining two (V3 and V4) are detached or semi-detached eclipsing binaries.

In the most recent survey for variable stars towards M71, Park & Nemec (2000) discovered a further 16 faint variables with

★ E-mail: jmcc@ing.iac.es

mean magnitudes within $15.2 < V < 20.3$, 8 of which are definite variables, 3 probable and 5 possible. As previous searches for variable stars in M71 were limited to small areas around the cluster centre, Park and Nemec primarily conducted their search in the outer regions (out to $r = 8.4$ arcmin from the cluster centre). They identified four possible new SX Phe-type stars (v9, v13, v16 and v22), two of which (v9 and v22) were discovered within 1 arcmin of the cluster centre. The 16 faint variables of Park & Nemec (2000) combined with the 7 previously discovered by Hodder et al. (1992) and Yan & Mateo (1994) gave a total of 4 known bright and 23 faint variables towards M71 prior to our study.

Whilst the goal of these GC photometric surveys was the detection of variable stars, for more recent surveys the detection of exoplanets has been the prime objective (e.g. 47 Tuc – Gilliland et al. 2000, Weldrake et al. 2005 and ω Cen – Weldrake, Sackett & Bridges 2008), although no evidence has been found for an exoplanet orbiting a star in a GC and the hot Jupiter occurrence rate in GCs remains unknown.

Several transiting exoplanet surveys have also been conducted of younger (age $\leq$ 4 Gyr), more metal-rich ($-0.23 \leq$ [Fe/H] ≤ 0.15) stars in open clusters (OCs), e.g. NGC 6819 (Street et al. 2003), NGC 6940 (Hood et al. 2005), NGC 7789 (Bramich et al. 2005), NGC 6791 (Mochejska et al. 2005), NGC 2158 (Mochejska et al. 2006), NGC 1245 (Burke et al. 2006) and Praesepe (Pepper et al. 2008). None of these surveys found significant evidence of transiting exoplanets. Recently, Quinn et al. (2012) discovered the first two giant planets orbiting main-sequence (MS) stars in the young (600 Myr) OC Praesepe using the radial velocity (RV) method, indicating that hot Jupiters do form and indeed survive in cluster environments.

Meibom et al. (2013) recently discovered the first two transiting exoplanets orbiting Sun-like stars in a cluster environment using data from the *Kepler* spacecraft. The planets, Kepler-66b ($R_p = 2.8$ $R_\oplus$, $P_{orb} = 17.8$ d) and Kepler-67b ($R_p = 2.9$ $R_\oplus$, $P_{orb} = 15.7$ d), were discovered in the extremely old (10^9 yr) OC NGC 6811 as part of the Kepler Cluster Survey (Meibom 2011). Meibom et al. (2013) find no significant difference between the occurrence rates of Neptune-sized planets inside and outside OCs. This strengthens the idea that such planets must be able to survive the high stellar densities and the violent deaths and high-energy radiation of massive stars, to which they were inevitably subjected during the early stages of cluster evolution. However, we note that the results of Meibom et al. (2013) are based on low number statistics and that the hot Jupiter occurrence rate in OCs may still differ somewhat from that around field stars. Continued monitoring of many more OCs is required to place more stringent limits on the occurrence rates of exoplanets, of all sizes, in OCs.

Previous surveys in M71 targeted different regions of the cluster with varying levels of photometric accuracy. The survey presented here aims to discover new variable stars and possibly transiting exoplanets in M71. The relatively high metallicity ([Fe/H] = −0.7; Smolinski et al. 2011) and lower stellar density of M71 also make it a more favourable host for planetary systems in comparison to other metal-poor, densely packed GCs. M71 also contains more stars than a typical OC, and its apparent diameter (∼7 arcmin) is matched well with the field of view (FOV) of the Near-Infrared Transiting ExoplanetS (NITES) telescope (∼11 arcmin × 11 arcmin, see Section 2) allowing the cluster to be imaged out to ∼63 per cent of its tidal radius $r_t = 8.96$ arcmin[1] (Harris 1996) in a single pointing. With the

NITES telescope we are able to search for lower amplitude, longer period variability than in previous surveys.

In Section 2, we introduce the NITES telescope, outline our observations of M71 and describe our data reduction processes. In Section 3, we describe our method of detecting stellar variability. In Section 4, we highlight our sensitivity to transiting hot Jupiters in M71 and present simulations of the expected number of detections. In Section 5, we summarize the results of our survey and comment on the apparent lack of RR Lyrae (RRL) variables in M71. In Section 6, we estimate spectral types and discuss cluster membership probabilities for the variable stars in M71. Finally, we close with a summary in Section 7. In Appendix A, we highlight the NITES telescope's photometric performance, comparing it to a theoretical noise model of the system.

2 THE NITES TELESCOPE, OBSERVATIONS AND DATA REDUCTION

The NITES telescope is an $f/10$ 0.4-m Meade LX200GPS[2] Schmidt–Cassegrain telescope. The CCD camera is a Finger Lakes Instrumentation (FLI)[3] Proline 4710 (hereafter PL4710) with a back-illuminated 1024×1024, 13 µm pixel, deep-depleted CCD made by e2v.[4] The deep depletion CCD suppresses fringing, has a peak quantum efficiency of QE >90 per cent around 800 nm and is sensitive out to 1 µm (where QE ≈ 25 per cent). The focal length of the telescope is 4064 mm which gives an FOV of 11.26 arcmin × 11.26 arcmin, and a plate scale 0.66 arcsec pixel^{-1}, respectively. Using a Peltier cooler, PL4710 runs at −40 °C; at this temperature dark current is noticeable at 3.11 e$^-$ pixel^{-1} s^{-1}. PL4710 can be read out at pixel rates of 0.75 or 2 MHz with resulting gains and read noises of 1.22 and 1.23 e$^-$ ADU^{-1}, and 8.8 and 14.0 e$^-$, respectively. During our survey of M71, the telescope focus was controlled using a basic system supplied by Meade. The focuser had no absolute position encoder and gave poor focusing repeatability. It has since been upgraded to an FLI Precision Digital Focuser (PDF). The PDF contains an absolute stepper motor, encoded with 7000 steps and a step size of 1.25 µm, allowing for more repeatable focus control. The telescope is mounted on a custom wedge made by Maurice Walsh & Co.,[5] Ballynahinch, UK. The wedge allows for more precise polar alignment over the traditional fixed pier system. The telescope and its control system are housed inside a 7 ft Astrohaven[6] clamshell dome which is located beside SuperWASP-North (Pollacco et al. 2006) at the Observatorio del Roque de los Muchachos on La Palma. Weather information is taken from the SuperWASP meteorological system in real time. The NITES telescope utilizes the DONUTS autoguiding algorithm (McCormac et al. 2013) which calculates guide corrections from the science images directly.

2.1 Photometry with the NITES telescope

Remote observations of M71 using the NITES telescope began on 2011 June 17 and continued until 2011 August 29; exposure times of 30 s were typically used. To increase the sensitivity of the survey, observations were made without a filter. In total, the survey collected

---

[1] http://physwww.mcmaster.ca/~harris/Databases.html

[2] http://www.meade.com
[3] http://www.flicamera.com
[4] e2v model 47-10, available at: http://www.e2v.com.
[5] http://www.mauricewalsh.com
[6] http://www.astrohaven.com
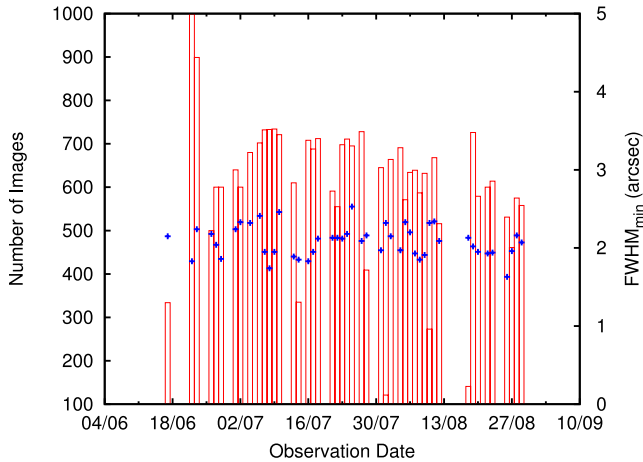
Figure 1. Summary of the NITES survey observations. The red boxes show the number of images acquired per night. Observations on the nights of 2011 June 22 and 23, where significantly more images were acquired, were made with 15 s exposure times. Observations on the other nights were made with 30 s exposure times. The blue crosses show the minimum FWHM in arcseconds for each night. The minimum FWHM was typically constrained by the lack of fine focus control rather than poor seeing. The focuser on the NITES telescope has since been upgraded.

data over a 74 d baseline with 47 nights of observations, equating to 228.3 h on sky, collecting 28 340 images. To monitor the seeing and focus variations during each run and from night to night, the median full width at half-maximum (FWHM) of each frame was measured using SEXTRACTOR (Bertin & Arnouts 1996). A summary of the observations is given in Fig. 1.

Data were reduced using standard routines in IRAF.[7] The reduced data from the entire survey were then batch processed using the difference-imaging software DIAPL2 (Pych, private communication). The software makes use of the method of Optimal Image Subtraction of Alard & Lupton (1998) and is an improved version of DIAPL (Wozniak 2000). DIAPL2 allows for the creation of smaller image subsections which treat rapidly varying point spread functions (PSFs) better.

DIAPL2 begins by measuring the average FWHM of all the images to be processed and ranks them in increasing order. The sharpest frames with the lowest background counts are ranked highest and are combined to create the template image of the field to which the others are compared. The highest ranked image is used as the geometric reference to which all other images are aligned. A total of 53 images met our selection criteria of FWHM < 1.98 arcsec (3 pixels) and sky background <370 e⁻ pixel⁻¹, for template creation. Undersampled images (FWHM < 2 pixels) were discarded. The template image was subsequently broken down into four subsections to allow for better PSF fitting and subtraction. Each science image was then split into the same number of subsections and its template subtracted.

SEXTRACTOR was used to extract all the sources in the template image with peak flux per pixel within the linear region of the CCD (<45 000 e⁻). Images taken at elevations <35° were not used due to dome vignetting, and those with focus drifts (median FWHM > 4.30) were also excluded from the analysis. Approx-

imately 8 per cent of the data were lost due to dome vignetting or focus drift. Aperture radii of 10.0, 8.0 and 6.0 pixels (6.6, 5.3 and 4.0 arcsec) were tested, and a final aperture radius of 6 pixels (4.0 arcsec) was chosen as it gave the lowest rms in the reduced light curves.

To estimate the *V*-band magnitude at peak brightness (V_{peak}) of the stars observed with the NITES telescope, 11 bright photometric standards from table 1 of AH71 (A1, U, N, A7, A5, Y, X, L, A3, C and A2) were used to transform the white light photometric system to Johnson *V*. As the survey was conducted in white light, no colour information was available making it impossible to convert precisely to Johnson *V*. The method above simply acts as an estimation of the brightness on a magnitude scale.

Mid-exposure times were converted to Heliocentric Julian Date (HJD) using the method of Eastman, Siverd & Gaudi (2010). The point-to-point photometric errors from DIAPL2 were systematically larger by a factor of ∼2 compared with those from SEXTRACTOR. As the errors from SEXTRACTOR were closer to those expected from typical CCD noise (see Appendix A), they were preferred, and the errors from DIAPL2 were scaled using

$$e_{i,j} = \frac{\delta_{i,j}}{\bar{\delta}_i} \times E_i, \tag{1}$$

where $e_{i,j}$ is the corrected error for star i at time j, $\delta_{i,j}$ is the error from DIAPL2 for star i at time j, $\bar{\delta}_i$ is the mean of the errors from DIAPL2 for star i and E_i is the error of star i in the reference frame as measured by SEXTRACTOR.

2.2 *BV* photometry with the Wide Field Camera

In order to obtain accurate colour information for all the stars surveyed by the NITES telescope, we obtained six *B*- and six *V*-band images of M71 during photometric conditions using the Wide Field Camera (WFC) on the Isaac Newton Telescope (INT) on 2013 April 5. The observations in each filter were dithered by 1 arcmin steps to cover the gaps between the WFC mosaicked CCDs. The WFC data were reduced using the data reduction package THELI (Erben et al. 2005), which bias subtracted and flat fielded each of the WFC's four CCDs independently.

As M71 is quite crowded, instrumental magnitudes were obtained using PSF fitting in DAOPHOT (Stetson 1987). The PSF was modelled using 25 bright and isolated stars spread over the FOV. Instrumental magnitudes for 27 185 stars in the field were obtained and transformed to the standard system using the photometry of GM00. The transformation was carried out using

$$v_0 = v_{\text{inst}} - (X_v \times Z_v), \tag{2}$$

$$b_0 = b_{\text{inst}} - (X_b \times Z_b), \tag{3}$$

$$V - v_0 = a(B - V) + c_v, \tag{4}$$

$$B - V = b(b_0 - v_0) + c_{bv}, \tag{5}$$

where v_{inst} and b_{inst} are instrumental magnitudes, X_v and X_b are the atmospheric extinction coefficients, Z_v and Z_b are the average airmass of the mosaic WFC image in each band, B and V are the magnitudes of GM00 on the standard system, b_0 and v_0 are the atmospheric extinction-corrected instrumental magnitudes, a and b are the transformation coefficients, and c_v and c_{bv} are the zero-points. As only a small range of airmass was sampled, the extinction terms X_v and X_b were assumed to be 0.2179 and 0.1036, respectively. These values were found by interpolating the results from the

---

[7] IRAF is distributed by the National Optical Astronomy Observatories, which are operated by the Association of Universities for Research in Astronomy, Inc., under cooperative agreement with the National Science Foundation.

atmospheric extinction study of La Palma by D. L. King[8] to the central wavelength of each filter ($B_{\lambda cen} = 4298$ Å and $V_{\lambda cen} = 5425$ Å).

We calculated $a = 0.0015 \pm 0.0782$, $b = 0.83 \pm 0.02$, $c_v = 0.58 \pm 0.10$ and $c_{bv} = 0.23 \pm 0.02$ for the transformations above. After the transformation, we found a systematic offset of $+0.128$ mag fainter for the WFC V magnitudes compared to those of GM00. After correcting the systematic offset, the magnitudes presented here are found to be in excellent agreement with GM00.

3 SEARCHING FOR STELLAR VARIABILITY

We used a Lomb–Scargle (LS; Lomb 1976; Scargle 1982; Press & Rybicki 1989) periodogram to search for stellar variability with periods in the range $0.000\,83 < P < 100$ d with frequency steps of $\Delta f = 0.002$ d^{-1}. For each periodogram, we estimated the power detection threshold corresponding to a false alarm probability (FAP) of 0.1 per cent, according to the number of independent frequencies N_{freq} used (see Cumming, Marcy & Butler 1999). We tested our FAP performing extensive simulations on a set of 1000 synthetic light curves free from astrophysical periodic signals, modelled using real NITES light curves (time stamps, data gaps, data length). Because our data contain real periods at the n and n/x periods (mostly caused by our window function), we also used the CLEAN (Roberts, Lehar & Dreher 1987) algorithm to confirm our period detection.

Additionally, light curves with significant (FAP ≤ 0.1 per cent) periodicity from our LS analysis were analysed further using phase dispersion minimization (PDM; Stellingwerf 1978). The range of periods searched with PDM were restricted to ± 0.1 per cent of the period detected by the LS and CLEAN analyses. It was found that PDM typically returned a better fitting period, especially in the case of non-sinusoidal variability. Variable stars displaying evidence of multiple periods were also analysed using a Fourier power spectrum in the PERIOD04 program (Lenz & Breger 2005). Breger et al. (1993) and Kuschnig et al. (1997) show that for a significant detection an signal-to-noise ratio (SNR) > 4 is required for a given peak in the power spectrum; hence, we adopt the same criterion in our multifrequency analysis (see Section 5.3). A recent comparison of period fitting algorithms by Graham et al. (2013) showed that different types of variability in data of differing quality – both in terms of time sampling and noise characteristics – may have their periodicity more efficiently recovered by different algorithms. Here we choose to concentrate on periodic variability (stellar pulsations, eclipsing binaries as well as transiting exoplanets) and hence adopt the traditional algorithms, LS and PDM, and box least squares (BLS; see Section 4.2) in the case of searching for transiting exoplanets. We note, however, that these algorithms are not perfect, e.g. the well-known half-period aliasing problem of eclipsing binaries when using an LS analysis.

The error on each period was calculated using a bootstrapping technique. A random number generator was used to randomly resample, with replacement, each unfolded light curve 500 times, resulting in a series of light curves in which several data points may have been selected more than once and others not at all. PDM was run on this series of resampled light curves and the error on the period was taken as the standard deviation in the spread of periods measured in the resampled series. In the case of eclipsing binaries showing ellipsoidal variations and/or secondary eclipses, the
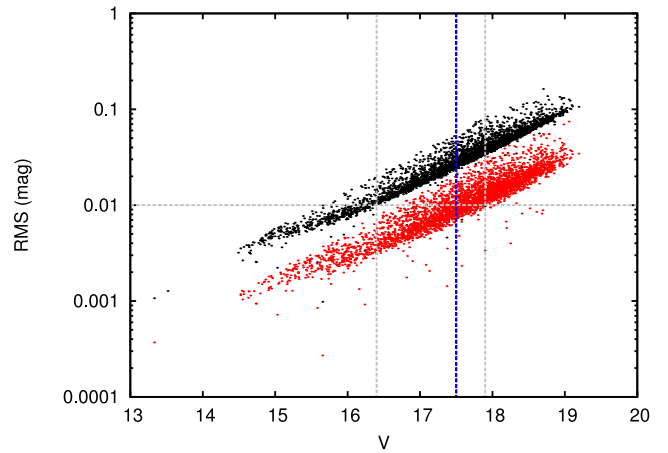
Figure 2. M71 rms versus V magnitude diagram from a typical night during the NITES survey (2011 August 04). The black points represent the unbinned data while the red points are from data binned into $\sim$6 min bins. The horizontal dashed grey line shows the 1 per cent accuracy level required to detect a 1 R_{Jup} sized planet. The vertical dashed grey lines show the limiting magnitudes at the 1 per cent level for the binned and unbinned data. The dashed blue line highlights the magnitude of the MSTO ($V = 17.5$) in M71.

strongest PDM period is often half the true orbital period. These light curves were easily identified by eye and their PDM period doubled.

4 DETECTABILITY OF TRANSITING HOT JUPITERS IN M71

To detect the transit of a typical hot Jupiter requires photometric precision at the 1 per cent level or better. Fig. 2 shows a typical rms versus magnitude diagram of M71 taken during dark time with the NITES telescope. The unbinned data from the night of 2011 August 04 (black points) are of insufficient accuracy around the main-sequence turn-off (MSTO, $V = 17.5$) to detect a transiting hot Jupiter. Fig. A1 shows that the NITES telescope is essentially free from correlated noise; hence, binning of our data points, as done by the BLS fitting algorithm (see Section 4.2), to increase our photometric accuracy is justified. The data from 2011 August 04 were subsequently binned 10-fold into $\sim$6 min bins and the rms versus magnitude diagram was recreated (see Fig. 2, red points). At this level of binning, it is clear that our variability survey is sensitive to transiting hot Jupiters at the top of the MS in M71. Since our survey only samples the bright end of the MS in M71, our targets are those with the least photon noise which allows for easier transit detection.

4.1 Transiting exoplanet expectations

In this section, we describe the process of creating a series of simulated NITES light curves containing hot Jupiter-like transits of differing depths and durations. The goal is to simulate the possible transit signals we might detect in our survey data and determine our detection success rate using the transit detection algorithm described in Section 4.2. Given the hot Jupiter period and median radius (3.235 d and 1.256 R_{jup}, August 2013; see exoplanet encyclopaedia[9]), we investigated our sensitivity in the case of a hot Jupiter with a period of $P = 3.2$ d and a radius $R_p = 1.3$ R_{jup}.

---

[8] http://www.ing.iac.es/Astronomy/observing/manuals/ps/tech_notes/tn031.pdf

[9] http://www.exoplanet.eu

Table 1. Simulated light curve parameters calculated using equations (6) and (7) and the estimates of stellar mass and radius of Bergbusch & VandenBerg (2001). The final column shows the number of stars in each magnitude bin of the NITES survey with rms < transit depth for a 1.3 R_{Jup} planet.

V (mag)	Transit depth (mag)	Transit duration (h)	rms$_{lim}$ (mag)	N_{stars}
17.50	0.010 74	2.79	0.007	210
17.75	0.013 69	2.48	0.009	255
18.00	0.016 35	2.29	0.011	268
18.25	0.019 42	2.12	0.013	189
18.50	0.022 80	1.97	0.017	115
18.75	0.026 17	1.86	0.022	36
19.00	0.029 58	1.76	0.030	1

We adopted the estimates for R_s and M_s as in 47 Tuc (see Bergbusch & VandenBerg 2001 and also Weldrake et al. 2005) for the simulations of exoplanet detectability presented here. Excluding the effects of limb darkening, the transit depth, δM, and duration, t_{trans}, in hours for the simulated light curves can be estimated using

$$\delta M \sim \left(\frac{R_p}{R_s} \right)^2, \tag{6}$$

$$t_{trans} = 1.412 \, M_s^{-1/3} \, R_s \, P^{1/3}, \tag{7}$$

where R_p and R_s in equation (6) are the radii of the planet and star, respectively, and M_s and R_s in equation (7) are the mass and radius of the star in solar units and P is the orbital period in days (Gilliland et al. 2000).

For a given V magnitude, each light curve was created with the depths and durations given in Table 1. The synthetic set spans the length of the survey with a time sampling of 0.0005 d, chosen in order to match the real NITES time sampling. The first mid-transit time for each individual light curve was randomly selected from the three days before our observing window. Gaussian noise was then added to individual light curves where the rms is the limiting accuracy of the NITES survey in each magnitude bin (see Table 1).

The synthetic light curves were compared to the real times of observation during the survey, and points which did not correspond to time on sky were excluded. As observations were carried out only when conditions were favourable, no explicit simulations of weather and observing conditions were performed. The process was repeated 50 times for each V magnitude bin (see Table 1), resulting in 350 simulated light curves with randomly occurring transits throughout. As can be seen in Table 1, the depths of any transits detectable by the NITES telescope are expected to range from ∼0.01 to 0.03 mag.

The simulated light curves were analysed with the BLS algorithm explained in Section 4.2. The expected transit depth in each magnitude bin from Table 1 was used to separate stars suitable for transit searching from those with insufficient photometric accuracy. The final column in Table 1 gives the total number of stars per magnitude bin with photometric precision better than the corresponding depth of a 1.3 R_{Jup} planet. A total of 1074 stars were observed on the MS of M71 down to $V \sim 19.0$ with sufficient accuracy to discover a transiting hot Jupiter.

There are currently conflicting numbers regarding the hot Jupiter occurrence rate around Sun-like stars in the solar neighbourhood. Wright et al. (2012) summarize the situation and show that the rate differs by up to a factor of 4 depending on the source. Results from
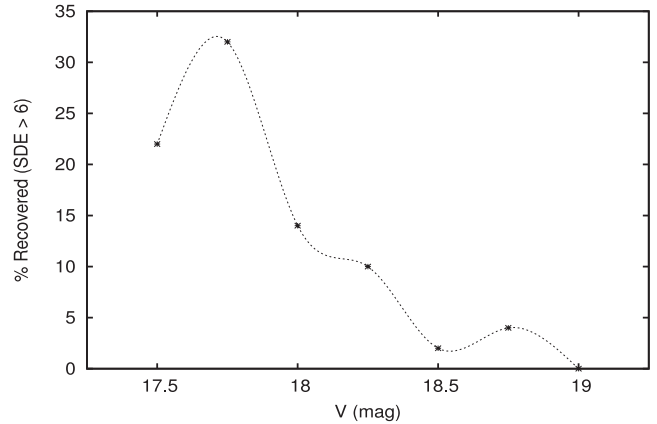
Figure 3. BLS detection efficiency per magnitude bin for a 1.3 R_{Jup} planet on a $P = 3.2$ d orbit. Detections are only assumed real if SDE > 6 (see Section 4.2).

the *Kepler* (Howard et al. 2012) and *OGLE-III* (Gould et al. 2006) transit surveys (adjusted for all orbital geometries, transiting and non-transiting) disagree with those from the RV surveys (Marcy et al. 2005; Cumming et al. 2008; Mayor et al. 2011; Wright et al. 2012) by a factor of 2–3. Wright et al. (2012) suggest that part of this may stem from the likely lower metallicity in the vicinity of the distant *Kepler* field objects. These distant objects will have significant heights above the Galactic plane, possibly separating the population from that of the RV surveys, by age and, potentially, metallicity. Beatty & Gaudi (2008) show that in the S/N-limited case (i.e. *Kepler*), the transit detection rate goes as R_p^6; hence, the properties of the RV and transit survey planets are considerably different, notably the larger radii and shorter orbital periods discovered by the transit surveys.

If we assume an average of only *Kepler* and *OGLE-III* occurrence rates, we would expect there to be four hot Jupiters per thousand MS stars. Assuming 10 per cent of those transit, we expect there to be 0.4 detectable transiting hot Jupiters in the NITES survey. Johnson et al. (2010) suggest that the giant planet occurrence rate is dependent on both the host star mass *and* metallicity. However, equation 8 of Johnson et al. (2010) does not account for the fraction of giant planets of short-period orbits. In reality, the likelihood of detecting a hot Jupiter on the MS of M71 depends on several factors – metallicity, stellar mass and orbital period – the details of which remain uncertain. This makes the search for transiting giant planets in M71 an interesting endeavour.

Using the BLS detection efficiencies shown in Fig. 3, we calculate an average of an ∼10 per cent chance of recovering a transiting hot Jupiter signal over the MS magnitude range $17.5 < V < 18.75$. No significant detections were returned from the synthetic light curve analysis at $V = 19.0$.

4.2 Transit detection method

The light curves were searched for transit signals using the BLS algorithm of Kovács, Zucker & Mazeh (2002). We searched for transit durations in the range $0.01 < t_{frac} < 0.1$ and periods in the range $0.5 < P < 10$ d in 2000 frequency steps of 0.0001 d^{-1}. The signal detection efficiency (SDE) was calculated for each BLS power spectrum using equation 6 of Kovács et al. (2002), and we assume the same criterion SDE > 6 to represent a significant detection.

5 RESULTS AND DISCUSSION

Our search for variable stars has discovered 17 new variables towards M71, and 7 of the previously proposed variables have been confirmed and had their periods determined or refined. The new variables all lie within the cluster's projected tidal radius $r_t = 8.96$ arcmin. They have been given numbers ranging from v24 to v40, in keeping with the nomenclature of Park & Nemec (2000, hereafter PN00). Section 5.1 highlights the results from our search for hot Jupiters in the NITES survey data. A brief description of only the remarkable – in the sense that their period or type of variability is found to be different here from that published in the literature – previously discovered variables (QU Sge, S4, v10 and v16) is given in Section 5.2. The details of the others (v1, v2, v3, v4, v5, v19, v20, v21 and v23) are summarized in Tables 2 and 3. Section 5.3 gives an overview of the new variable stars discovered here (v24–v40). Folded light curves for those with a single periodicity detected are shown in Figs 4 and 5. For clarity, the light curves have been averaged into bins of 0.001 in phase and the error bars have been excluded. Figs 6 and 7 show the light curves of the multiply periodic variables v26, v27, v28, v31, v34, v35, v36 and v40. For clarity, in Figs 6 and 7 the data points have been averaged into 50 bins per night and the error bars have also been excluded. A summary of the frequencies detected in the multiply periodic variables is given in Table 4 . A finding chart for each of the new variables is given in Fig. 8. We would like to note that it is notoriously difficult to perform precise photometry in crowded stellar environments and in the presence of saturated stars located close to variable objects (e.g. Scottfelt et al. 2013). The inevitable effects of blending may influence to a certain degree the amplitude and/or the period of variable stars in crowded areas or regions surrounding saturated objects.

5.1 Transiting hot Jupiters towards M71

A total of 1074 light curves were flagged as having sufficient photometric accuracy to detect a 1.3 $R_{\rm Jup}$ planet on a 3.2 d orbit and were analysed using the BLS method above. A total of five objects showed significant detections (SDE > 6), two of which are variable stars (v28 and v30; see Section 5.2) and one is a probable eclipsing binary of PN00 (v10; confirmed here in Section 5.3). The

Table 2. Summary of the new and previously discovered variables observed in the NITES survey. The distance from the cluster centre r_c in arcseconds was calculated for each star using the cluster centre coordinates RA (J2000) 19^h 53^m 46^s and Dec. (J2000) +18° 46′ 40″ of PN00. ΔV is the peak-to-peak change in brightness in magnitudes and $N_{\rm obs}$ is the final number of reduced observations analysed for each target. The periods for multiply periodic variables are the principal periods detected. A period improvement is defined as yes if it has been newly determined here or significantly refined with respect to previously published values. DB: detached binary; SD: semi-detached binary; CB: contact binary; EB: eclipsing binary of undefined type; δ Sct-like: δ Scuti-like variable star; LP: long-period variable of undefined type; SR: semi-regular type variable; MP: multiply periodic.

Star	RA (J2000)	Dec. (J2000)	r_c (arcsec)	ΔV (mag)	$N_{\rm obs}$	Period (d)	$P_{\rm err}$ (d)	Period improved	Variable type
Previously discovered:									
QU Sge	19^{h}53^{m}49^{s}34	+18°45′43″26	74.0	0.892	23 466	3.791 00	0.000 61	No	SD / MP
S4	19^{h}54^{m}04^{s}91	+18°47′24″55	272.2	0.367	22 229	2.525 252	0.000 033	Yes	DB
v1	19^{h}53^{m}57^{s}49	+18°43′33″76	247.6	0.573	23 243	0.348 904	0.000 025	No	CB
v2	19^{h}53^{m}57^{s}09	+18°45′46″97	166.2	0.357	23 213	0.367 21	0.000 01	No	CB
v3	19^{h}53^{m}50^{s}84	+18°47′51″48	99.2	0.168	23 238	0.373 856	0.000 018	No	CB
v4	19^{h}53^{m}49^{s}34	+18°47′49″70	84.3	0.096	23 206	0.556 15	0.000 02	No	DB
v5	19^{h}53^{m}34^{s}28	+18°44′05″01	227.4	0.373	23 240	0.404 341	0.000 015	No	CB
v10	19^{h}54^{m}01^{s}76	+18°47′16″73	226.8	0.106	21 642	0.796 674	0.000 033	Yes	CB?
v16	19^{h}53^{m}58^{s}96	+18°49′28″48	249.5	0.062	23 227	0.642 204	0.000 047	Yes	CB?
v19	19^{h}54^{m}09^{s}60	+18°47′21″78	337.7	0.594	23 174	6.1070	0.0042	Yes	EB?
v20	19^{h}53^{m}23^{s}44	+18°42′10″61	418.6	0.540	9 585	0.469 967	0.000 028	Yes	CB
v21	19^{h}53^{m}25^{s}54	+18°51′17″44	401.7	0.330	23 129	0.357 907	0.000 005	Yes	CB
v23	19^{h}53^{m}57^{s}68	+18°42′50″67	283.0	0.602	23 293	5.657 241	0.000 027	Yes	DB
Newly discovered:									
v24	19^{h}54^{m}08^{s}11	+18°42′13″41	412.0	0.936	23 268	1.336 73	0.000 29	Yes	DB
v25	19^{h}53^{m}46^{s}43	+18°46′46″01	8.6	0.033	22 690	11.663 32	0.000 56	Yes	EB?
v26	19^{h}53^{m}47^{s}94	+18°49′37″19	179.3	0.045	23 223	0.413 481	0.000 052	Yes	δ Sct-like/MP
v27	19^{h}53^{m}51^{s}48	+18°46′00″53	87.3	0.020	23 466	3.5582	0.0012	Yes	δ Sct-like/MP
v28	19^{h}53^{m}28^{s}40	+18°41′45″31	386.5	0.013	23 137	0.082 964	0.000 002	Yes	δ Sct-like/MP
v29	19^{h}53^{m}42^{s}72	+18°45′58″35	62.5	0.070	23 245	0.190 207	0.000 017	Yes	δ Sct-like
v30	19^{h}53^{m}53^{s}08	+18°47′14″36	106.3	0.030	23 190	0.166 267	0.000 018	Yes	δ Sct-like
v31	19^{h}54^{m}02^{s}86	+18°42′50″31	331.8	0.112	17 153	2.4452	0.0011	Yes	EB?/MP
v32	19^{h}54^{m}07^{s}41	+18°43′04″73	372.6	0.174	23 355	48.178	0.021	Yes	LP
v33	19^{h}53^{m}28^{s}62	+18°44′05″73	291.1	0.181	23 240	5.418 895	0.000 18	Yes	LP
v34	19^{h}53^{m}41^{s}39	+18°44′44″41	132.8	0.043	22 962	45.8295	0.0056	Yes	MP
v35	19^{h}53^{m}45^{s}09	+18°43′01″35	219.0	0.114	22 486	54.884 70	0.000 56	Yes	SR?/MP
v36	19^{h}54^{m}11^{s}28	+18°52′01″56	481.9	0.098	19 828	22.5377	0.0016	Yes	SR?/MP
v37	19^{h}53^{m}48^{s}95	+18°47′13″76	53.8	0.080	20 905	24.046 35	0.000 83	Yes	LP
v38	19^{h}54^{m}05^{s}44	+18°51′58″36	421.3	0.067	22 695	–	–	–	LP
v39	19^{h}53^{m}38^{s}34	+18°49′25″33	197.9	0.021	22 732	11.182 42	0.000 51	Yes	LP
v40	19^{h}53^{m}41^{s}90	+18°51′24″81	290.7	0.147	20 932	26.860 00	0.000 62	Yes	SR?/MP

Table 3. Summary of variable star parameters. Intrinsic V_0 magnitudes and $(B - V)_0$ colours for 38 of the 40 variable stars towards M71 calculated using the reddening measurements of Schlegel et al. (1998) and $A_V/E(B - V) = 3.1$. Stars v6 and v7 could not be identified with confidence in our WFC data. The range of spectral types have been estimated using the transformations of Schmidt-Kaler (1982). We note that the specific spectral type of each object depends upon the determination of its luminosity class, which in turn requires a full spectroscopic classification not carried out here. In the Notes column, the distances (d in kpc) to the short-period δ Scuti-type variables are calculated using V_0 from Column 1 and equation 1 of McNamara (2011), and the cluster membership probabilities (p per cent) are those from the proper motion survey of CW85.

Star	V_0 (mag)	$(B - V)_0$ (mag)	$E(B - V)$ (mag)	Spectral type	Notes
Previously discovered:					
QU Sge	14.321 ± 0.018	0.290 ± 0.019	0.309 ± 0.015	F0	$d = 1.68 \pm 0.07, p = 51$ per cent
S4	13.704 ± 0.013	0.418 ± 0.014	0.306 ± 0.011	F4/F5	$p = 0$ per cent
v1	17.212 ± 0.017	0.634 ± 0.020	0.300 ± 0.012	G0/G2	
v2	16.755 ± 0.017	0.573 ± 0.160	0.306 ± 0.012	G0/F9	
v3	18.190 ± 0.035	0.930 ± 0.057	0.316 ± 0.016	G8/K2	
v4	16.449 ± 0.021	0.534 ± 0.024	0.313 ± 0.016	F8	
v5	17.119 ± 0.022	0.588 ± 0.025	0.329 ± 0.019	F9/G0	
v8	17.830 ± 0.026	0.689 ± 0.031	0.299 ± 0.014	G1/G5	
v9	16.683 ± 0.027	0.434 ± 0.031	0.311 ± 0.015	F5	
v10	14.359 ± 0.014	1.236 ± 0.014	0.306 ± 0.012	K3/K6	
v11	19.129 ± 0.045	0.828 ± 0.079	0.312 ± 0.012	G4/K0	
v12	17.401 ± 0.032	0.856 ± 0.037	0.344 ± 0.023	G5/K1	
v13	16.210 ± 0.029	0.385 ± 0.031	0.429 ± 0.027	F3	
v14	17.511 ± 0.029	0.582 ± 0.033	0.340 ± 0.024	F9/G0	
v15	17.359 ± 0.028	0.590 ± 0.031	0.336 ± 0.022	F9/G0	
v16	15.744 ± 0.016	0.416 ± 0.017	0.324 ± 0.014	F4	
v17	18.277 ± 0.045	0.659 ± 0.061	0.332 ± 0.016	G0/G4	
v18	18.630 ± 0.031	0.705 ± 0.045	0.291 ± 0.014	G1/G6	
v19	18.184 ± 0.026	0.955 ± 0.042	0.302 ± 0.012	G9/K3	
v20	15.419 ± 0.022	0.454 ± 0.023	0.324 ± 0.021	F6	
v21	15.028 ± 0.034	0.585 ± 0.036	0.397 ± 0.030	F9/G0	
v22	15.586 ± 0.016	0.417 ± 0.019	0.309 ± 0.015	F4	$p = 15$ per cent
v23	15.666 ± 0.015	0.622 ± 0.016	0.297 ± 0.012	F9/G2	
Newly discovered:					
v24	17.054 ± 0.019	0.411 ± 0.021	0.284 ± 0.015	F4	
v25	14.044 ± 0.019	0.772 ± 0.019	0.326 ± 0.018	G2/G9	
v26	14.461 ± 0.022	0.743 ± 0.023	0.338 ± 0.021	G2/G8	$d = 8.56^{+0.29}_{-0.28}$
v27	14.159 ± 0.016	0.759 ± 0.018	0.309 ± 0.014	G2/G9	$d = 10.75^{+0.36}_{-0.35}$
v28	12.550 ± 0.020	0.329 ± 0.021	0.328 ± 0.020	F1	$d = 1.40^{+0.05}_{-0.05}$
v29	17.502 ± 0.032	0.596 ± 0.037	0.311 ± 0.018	F9/G1	$d = 22.17^{+0.80}_{-0.77}$
v30	17.146 ± 0.022	0.483 ± 0.026	0.313 ± 0.015	F6/F7	$d = 17.41^{+0.60}_{-0.58}$
v31	11.999 ± 0.015	0.782 ± 0.016	0.293 ± 0.014	G2/G9	
v32	16.234 ± 0.016	0.819 ± 0.018	0.293 ± 0.014	G4/K0	
v33	15.342 ± 0.021	0.643 ± 0.022	0.340 ± 0.021	G0/G3	
v34	14.160 ± 0.016	0.853 ± 0.017	0.316 ± 0.016	G5/K1	$p = 0$ per cent
v35	13.891 ± 0.015	1.242 ± 0.015	0.303 ± 0.014	K3/K6	
v36	12.966 ± 0.021	1.299 ± 0.021	0.324 ± 0.013	K3/K7	
v37	14.008 ± 0.018	0.813 ± 0.018	0.326 ± 0.017	G4/K0	$p = 79$ per cent
v38	14.287 ± 0.020	0.760 ± 0.021	0.321 ± 0.013	G2/G9	
v39	14.005 ± 0.026	0.554 ± 0.027	0.346 ± 0.026	F8/F9	
v40	13.126 ± 0.031	1.314 ± 0.031	0.360 ± 0.029	K4/K7	

remaining two when folded on the detected period showed none of the characteristics of a transiting hot Jupiter: shallow, flat-bottomed and short-duration transits with respect to the period of variability. Although our sample is of more than 1000 stars, in order to place robust statistical constraints on the hot Jupiter frequency in a relatively metal-rich GC, a much larger sample of the cluster's MS is required.

5.2 Previously discovered variables towards M71

QU Sge is a semi-detached Algol-type eclipsing binary containing an SX Phe-type component discovered by Jeon et al. (2006). This was the first pulsating component of an eclipsing binary found in a GC. Jeon et al. (2006) refined the orbital period of QU Sge to $P = 3.790\,818 \pm 0.000\,012$ d. The eclipsing binary light curve was subtracted from the data revealing short-period ($P \sim 0.03$ d)
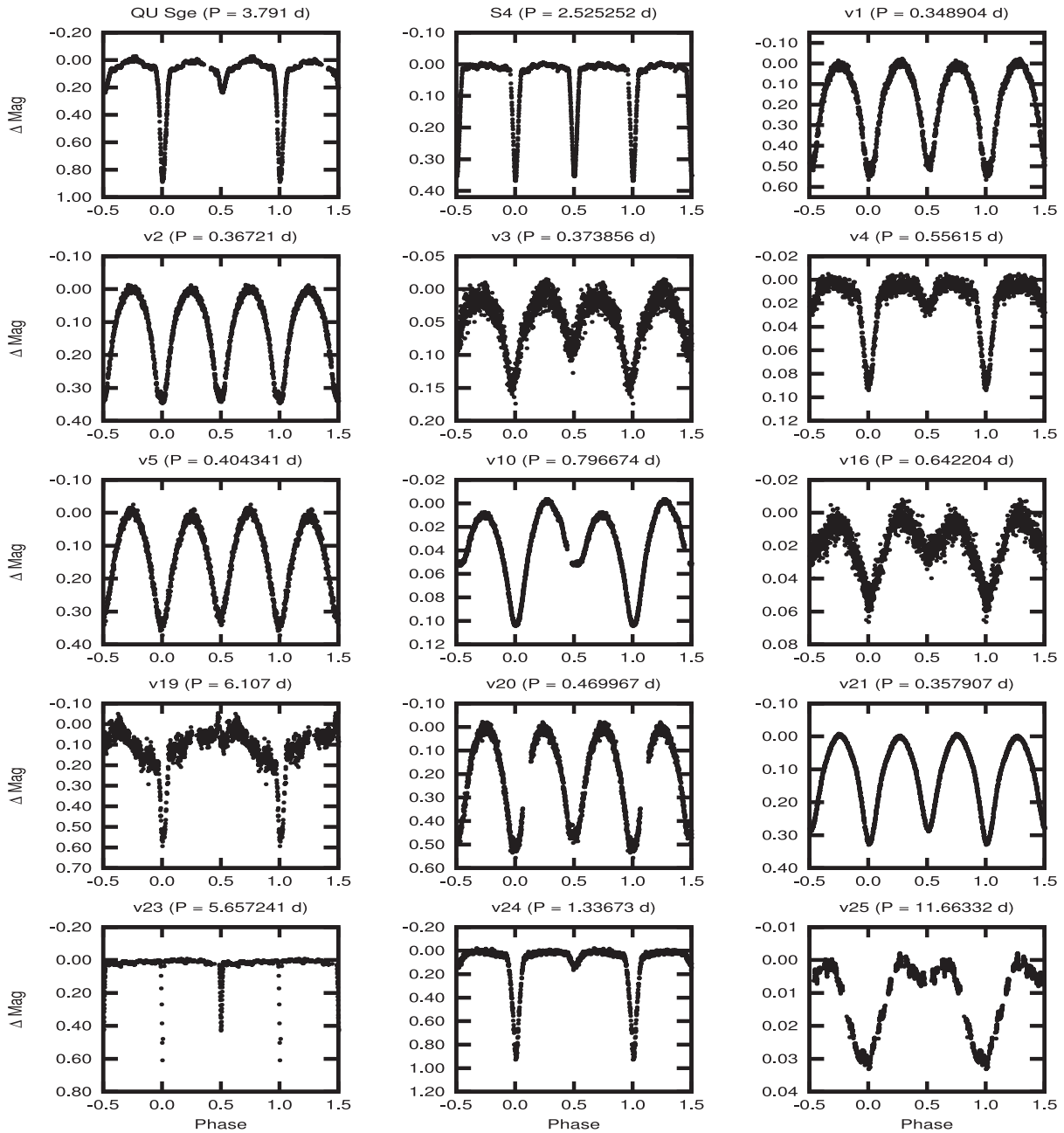
Figure 4. Folded light curves for the singly periodic, previously known variable stars QU Sge, S4, v1, v2, v3, v4, v5, v10, v16, v19, v20, v21 and v23, the newly confirmed Algol-type eclipsing binary v24 and the newly discovered eclipsing binary v25. The periods of S4, v10, v16, v19, v20, v21 and v23 have been improved through the analysis here; v23 is also confirmed as an Algol-type eclipsing binary. PN00 suggested that v16 could be an SX Phe-type variable but from the analysis presented here it appears to be an eclipsing binary.

low-amplitude (∼0.024 mag) variations which are consistent with SX Phe-type variability. Jeon et al. (2006) find two peaks in the power spectrum of QU Sge, $f_1 = 35.883$ cycles d^{-1} and $f_2 = 39.867$ cycles d^{-1}. As the ratio of the frequencies detected is larger than 0.8 [typical value for fundamental and first overtone modes assumed by Jeon et al. (2006)], they conclude that at least one of the two periods originates in a non-radial mode.

A period of $P = 3.79100 \pm 0.00061$ d for the eclipses of QU Sge (see Fig. 4) was found here, which is in agreement with the period $P = 3.790818$ d of Jeon et al. (2006). Nightly inspection of our QU Sge light curves also showed SX Phe-type variations. Non-eclipsing data were normalized with a second-order polynomial and

converted to differential magnitudes to highlight the variability. The results are shown in Fig. 9. The out-of-eclipse data were analysed collectively using a Fourier analysis. We find a non-equally spaced triplet in the power spectrum of QU Sge, with $f_1 = 33.9167$ cycles d^{-1}, $f_2 = 36.1381$ cycles d^{-1} and $f_3 = 38.8864$ cycles d^{-1}, two of which are similar to those of Jeon et al. (2006; see Fig. 9). The fundamental period of high-amplitude ($\Delta V \approx 0.2 - 0.3$) δ Scuti stars is shorter than the first overtone pulsation period by a factor of 0.775 (Poretti et al. 2005). The frequency ratios, $f_1/f_2 = 0.9385$, $f_1/f_3 = 0.8722$ and $f_2/f_3 = 0.9293$, from our analysis are also larger than 0.775, hinting that at least two of the detected periods originate from non-radial modes.
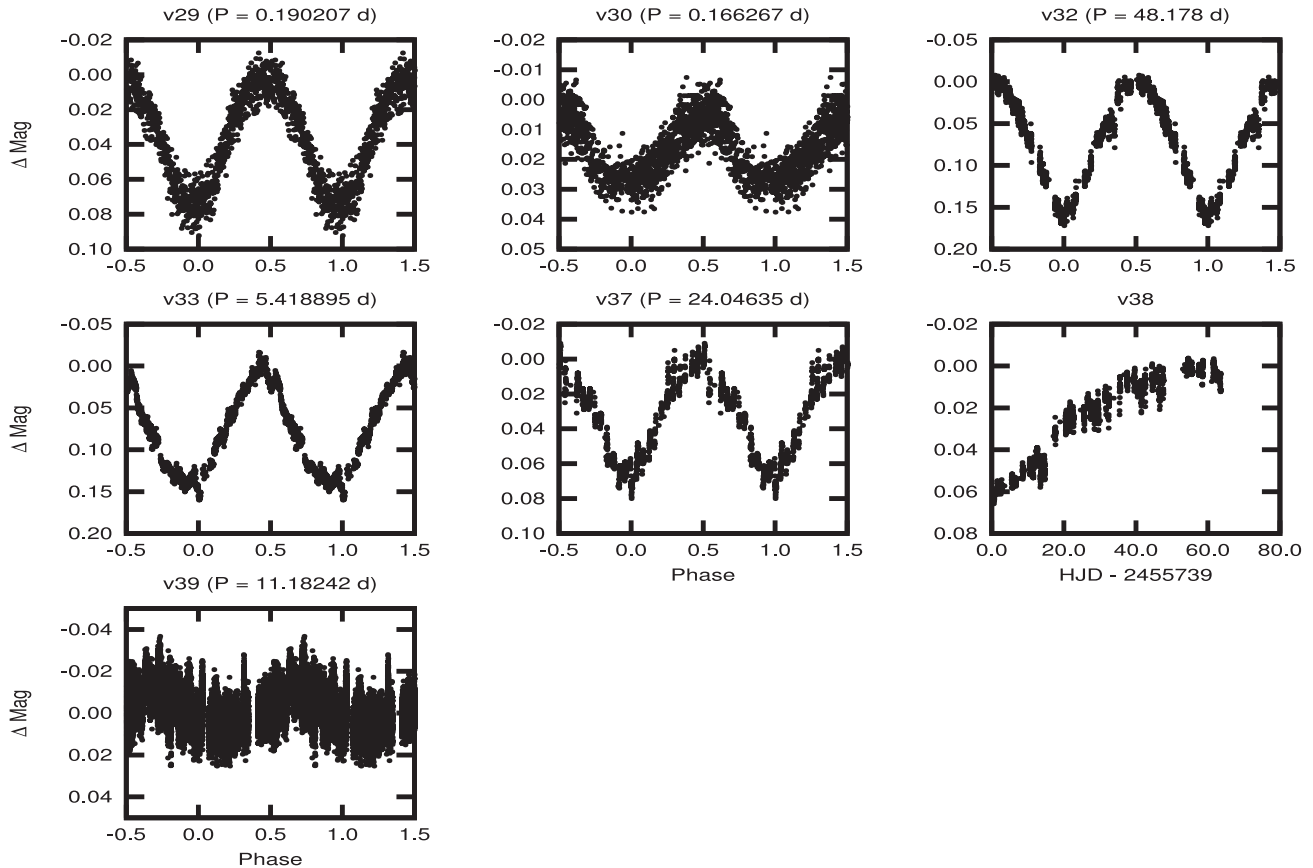
Figure 5. Folded light curves for the newly discovered, singly periodic δ Scuti-like variable stars v29 and v30, and the variable stars v32, v33, v37, v38 and v39. No significant periodicity could be determined for the variable v38 as less than one full cycle has clearly been observed. v39 displays large scatter in the data points on a nightly basis; the long-term periodic variations are more clearly seen unbinned.

The amplitude of the variations observed here is much larger, ∼0.2 mag compared to 24 mmag of Jeon et al. (2006) and is seen to vary over time (see Fig. 9). The greater amplitude observed here is likely caused by the modulation of the light curve by the three different, but closely separated frequencies. The difference in photometric bands between our observations and those of Jeon et al. (2006) (white light versus *V*) may also contribute to the differences observed in pulsation amplitudes. Assuming that we have detected radial pulsations and the fundamental frequency, we use the period–luminosity relation of McNamara (2011, their equation 1) to estimate the distance to QU Sge. We find $d = 1.68 \pm 0.07$ kpc, which places QU Sge in the foreground of M71 and agrees with the marginal cluster membership probability (51 per cent) of Cudworth (1985). If the first overtone has been detected, the distance above will be shorter by ∼15 per cent.

Our NITES observations of several other previously known variables have revealed some interesting results. S4 was originally proposed to be an RRL variable by Sawyer Hogg (1973); however, it actually appears to be a detached eclipsing binary with a period of $P = 2.525\,252 \pm 0.000\,033$ d, see Fig. 4. v10 was discovered by PN00 as a possible W UMa-type contact binary system with a period of $P = 0.768\,42$ d. However, the period found here ($P = 0.796\,674 \pm 0.000\,033$) differs significantly from that of PN00 by ∼41 min. PN00 quote no errors on the period of v10. We suspect that the difference most likely stems from their incomplete phase coverage of their observations, see Fig. 4. Finally, the variable star v16 was suggested to be an SX Phe-type variable by PN00. Our NITES observations show v16 to have variations of dif-

fering depths, see Fig. 4. v16 therefore appears to be a possible contact binary rather than an SX Phe variable.

5.3 New variables towards M71

v24: the first new eclipsing binary system found in the direction of M71 in over 10 years. We find a period using PDM of $P = 1.336\,73 \pm 0.000\,29$ d. v24 appears to be a detached eclipsing binary system with a primary eclipse depth approximately twice as large as the secondary (see Fig. 4).

v25: a possible long-period grazing eclipsing binary (see Fig. 4). Using PDM we find a period of $P = 11.663\,32 \pm 0.000\,56$ d. v25 is located in a very crowded region towards the centre of M71 (see Fig. 8). This combined with its relatively long period and shallow eclipse depth (∼30 mmag) may explain why it was previously undetected. A possible X-ray active binary candidate s07 (Elsner et al. 2008; Huang et al. 2010) is located 1.13 arcsec from v25 and its position is encompassed in the photometry aperture.

v26: a short-period, low-amplitude variable with a best-fitting period of $P = 0.413\,70 \pm 0.000\,05$ d, found using an LS periodogram. This object appears to be a δ Scuti-type variable but as its metallicity has not been determined here we cannot definitively distinguish between SX Phe and δ Scuti variations. For now we name v26 and the following four variables (v27, v28, v29 and v30), δ Scuti-like variable stars. Fourier analysis of v26 returns two significant (SNR > 4) peaks in the power spectrum $f_1 = 2.418\,49$ and $f_2 = 2.006\,66$ cycles d^{-1} (see Fig. 6).
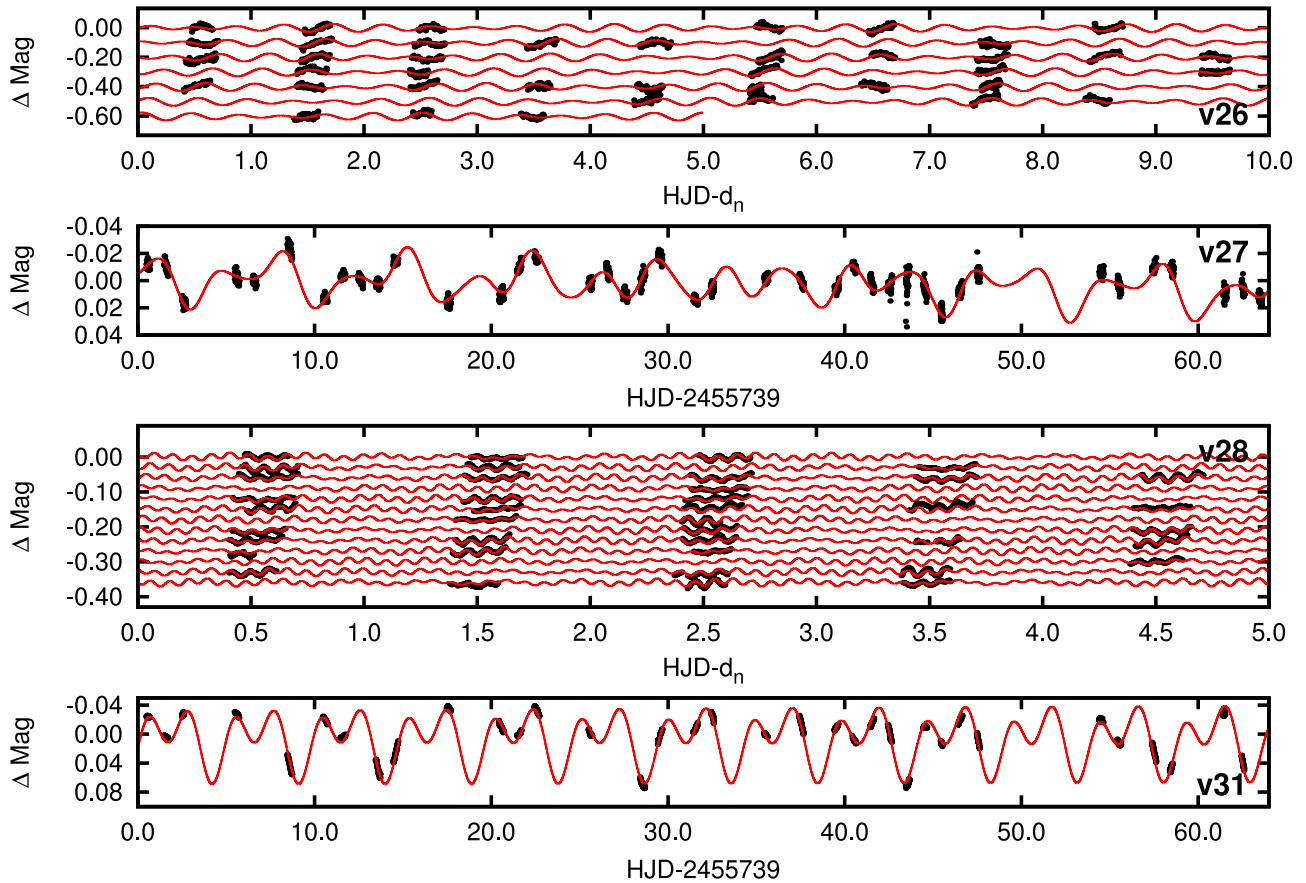
Figure 6. Light curves for the multiply periodic variables v26, v27, v28 and v31, overplotted with the best-fitting models from the Fourier analyses. The data have been combined into 50 binned points per night. For clarity, the data for v26 and v28 are shown in groups of 10 and 5 nights (starting at HJD 245 5739, where d_n is the Julian Day for a given night), and each group of nights have been offset by integer numbers of 0.10 and 0.03 mag, respectively. The significant frequencies detected for each object are given in Table 4.

v27: a low-amplitude, δ Scuti-like variable. We find a period of $P = 3.571\,429 \pm 0.001\,23$ d using an LS periodogram. When folded on this period v27 appeared to vary irregularly. Nightly inspection of the data showed variations on a shorter time-scale. v27 was folded on the next significant period, $P = 0.779\,27 \pm 0.000\,27$ d, where it shows regular, low-amplitude δ Scuti-like variations. A further two possible X-ray active binary candidates s27a and s27b (Elsner et al. 2008; Huang et al. 2010) are located 0.03 and 0.72 arcsec from v27, respectively. Given the small angular separation, we believe v27 to be X-ray binary candidate s27a. Fourier analysis of v27 returned many peaks with slightly reduced significance ($3 < \mathrm{SNR}_{f_n} < 4$) which could indicate aperiodic variability. Regardless, Fig. 6 shows the variations of v27 along with the best-fitting model created using the three most significant peaks $f_1 = 0.281\,04$ and $f_2 = 0.141\,95$ cycles d^{-1}. Although f_1 and f_2 appear to be multiples of one another, phasing upon either period individually results in a poorer fitting model.

v28: a δ Scuti-like low-amplitude variable. The strongest peak in the LS periodogram of v28 was found at $P = 0.082\,959 \pm 0.000\,002$ d. The δ Scuti-like variations are also visible on a nightly basis with this period. v28 is the shortest period δ Scuti-like variable discovered here, with a period within $-1.47 < \log P < -0.90$ d suggesting that it could possibly be an SX Phe-type variable (McNamara 2011). Fourier analysis of v28 returned three significant ($\mathrm{SNR} > 4$) peaks in the power spectrum $f_1 = 12.053\,47$, $f_2 = 3.006\,24$ and $f_3 = 11.618\,58$ cycles d^{-1} (see Fig. 6).

v29: a larger amplitude ($\Delta V \sim 0.07$ mag) δ Scuti-like variable (see Fig. 5). We find a best-fitting period of $P = 0.190\,207 \pm 0.000\,017$ d using PDM. Variations on this period are clearly visible in a night-by-night inspection of the data.

v30: the final δ Scuti-like variable discovered here. We find a period of $P = 0.166\,267 \pm 0.000\,018$ d using PDM. v30 was seen to vary only on the nights towards the end of the observing campaign and requires additional observations to confirm the type of variability (see Fig. 5).

v31: a possible eclipsing binary with asymmetrical eclipses. Using PDM we find a best-fitting period of $P = 4.8940 \pm 0.0011$ d. Analysis of the Fourier power spectrum of v31 returned peaks at $f_1 = 0.408\,96$ and $f_2 = 0.203\,67$ cycles d^{-1}. Similarly to v27, f_1 and f_2 appear to be multiples of each other but both frequencies are required to fit the double-peaked variation shown in Fig. 6.

v32: a relatively faint long-period variable star of undefined type (see Fig. 5). We find a best-fitting period of $P = 48.1782 \pm 0.0206$ d using PDM. It is possible that less than one full cycle of this star has been measured.

v33: a long-period variable star of undefined type (see Fig. 5). We detect a significant period at $P = 5.418\,895 \pm 0.000\,18$ d using an LS periodogram.

v34: a possible long-period eclipsing binary. Analysis of v34 using a Fourier power spectrum returns three significant frequencies $f_1 = 0.021\,82$, $f_2 = 0.041\,91$ and $f_3 = 2.009\,60$ cycles d^{-1} (see Fig. 7). v34 also displays short-period variations, however the periods of
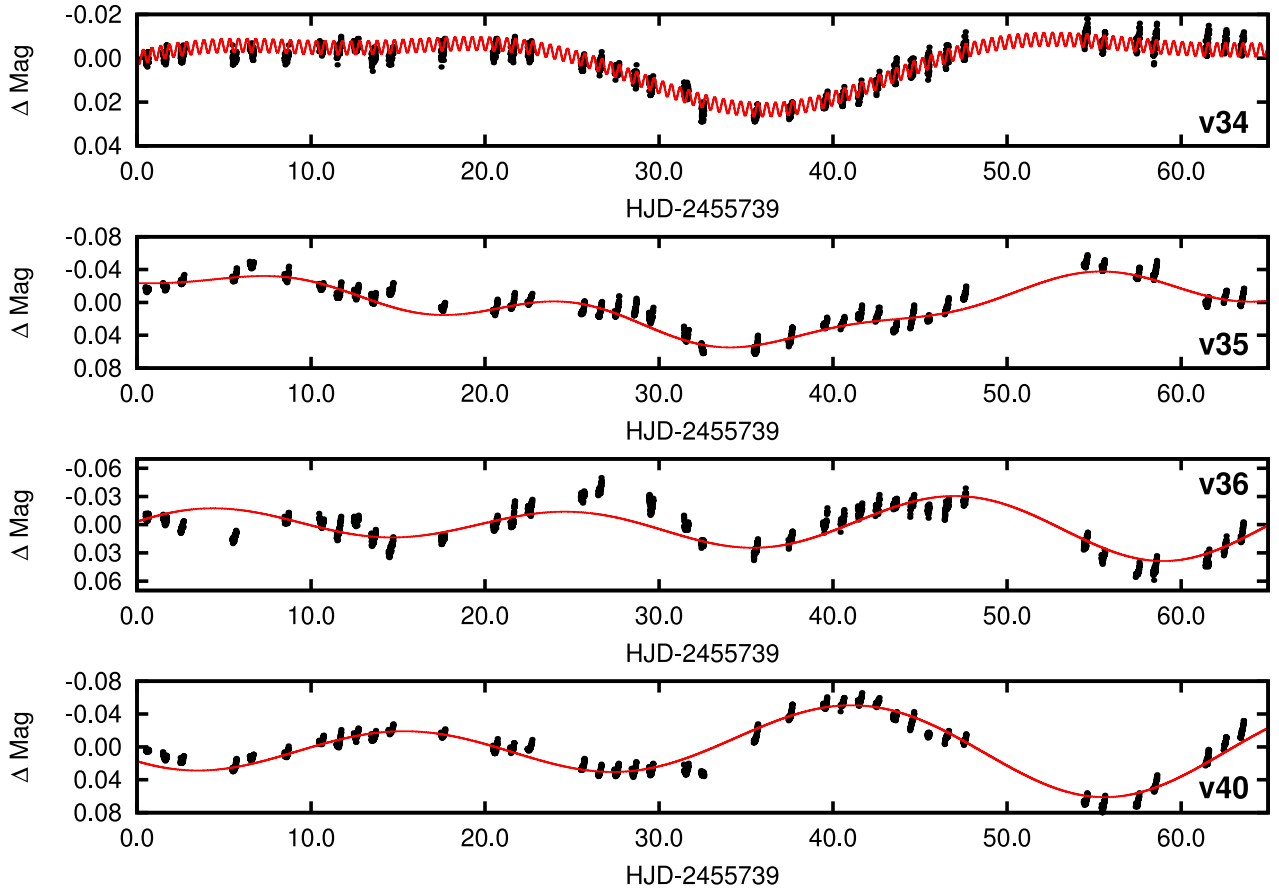
Figure 7. Light curves for the multiply periodic variables v34, v35, v36 and v40, overplotted with the best-fitting models from the Fourier analyses. The data have been combined into 50 binned points per night. The significant frequencies detected for each object are given in Table 4.

Table 4. A summary of the significant frequencies detected in the multiperiodic light curves of nine stars observed during the NITES survey of M71. All except QU Sge are newly discovered here.

Star	f_1 (cycles d^{-1})	f_2 (cycles d^{-1})	f_3 (cycles d^{-1})
QU Sge	33.9167	36.1381	38.8864
v26	2.418 49	2.006 66	–
v27	0.281 04	0.141 95	–
v28	12.0535	3.006 24	11.618 58
v31	0.408 96	0.203 67	–
v34	0.021 82	0.041 91	2.009 60
v35	0.018 22	0.064 96	0.039 61
v36	0.044 37	0.034 07	–
v40	0.037 23	0.025 34	–

which could not be detected with any significance. v34 appears to be the most complexly variable system discovered here.

v35: a long-period, possible semi-regular variable. v35 is much brighter than the MS in M71 and is possibly a pulsating giant or a field star. Fourier analysis of v35 returns several significant (SNR > 4) peaks in the power spectrum $f_1 = 0.018\,22$, $f_2 = 0.064\,96$ and $f_3 = 0.039\,61$ cycles d^{-1}. The light curve of v35 appears to be best fitted by a combination of them all (see Fig. 7).

v36: a bright variable star of undefined type. Our LS analysis returned a period of $P \sim 20$ d. A search for aliases around this period showed that not all the variations were of equal strength. The power spectrum of v36 shows two significant peaks at $f_1 = 0.044\,37$ and $f_2 = 0.034\,07$ cycles d^{-1}. It is clear that the object is variable (see Fig. 7) but the nature of the variability is uncertain. Further observations are required to constrain any periodicity.

v37: a long-period variable star of undefined type (see Fig. 5). We find a best-fitting period of $P = 24.046\,35 \pm 0.000\,83$ d. The X-ray binary s20 (Elsner et al. 2008; Huang et al. 2010) is located 0.07 arcsec from v37 and encompassed by the photometry aperture.

v38: a very long period variable, possibly the longest detected here (see Fig. 5). We find one significant peak ($f_1 = 0.005\,32$ cycles d^{-1}, $P \approx 188$ d) in the Fourier power spectrum of v38; however, this is much longer than the length of the NITES survey and constraining its period is therefore impossible. Continued observation of v38 is required to constrain the period.

v39: a long-period low-amplitude variable of undefined type. A best-fitting period of $P = 11.182\,42 \pm 0.000\,51$ d was found using an LS periodogram. The data show a large intra-nightly scatter, and binning masks the smooth long-term variations seen unbinned (see Fig. 5).

v40: a possible semi-regular variable. Analysis of the power spectrum of v40 reveals two significant peaks at $f_1 = 0.037\,23$ and $f_2 = 0.025\,34$ cycles d^{-1} (see Fig. 7). It appears from Fig. 7 that additional frequencies are present in v40 but are not detected with sufficient significance in our survey data.
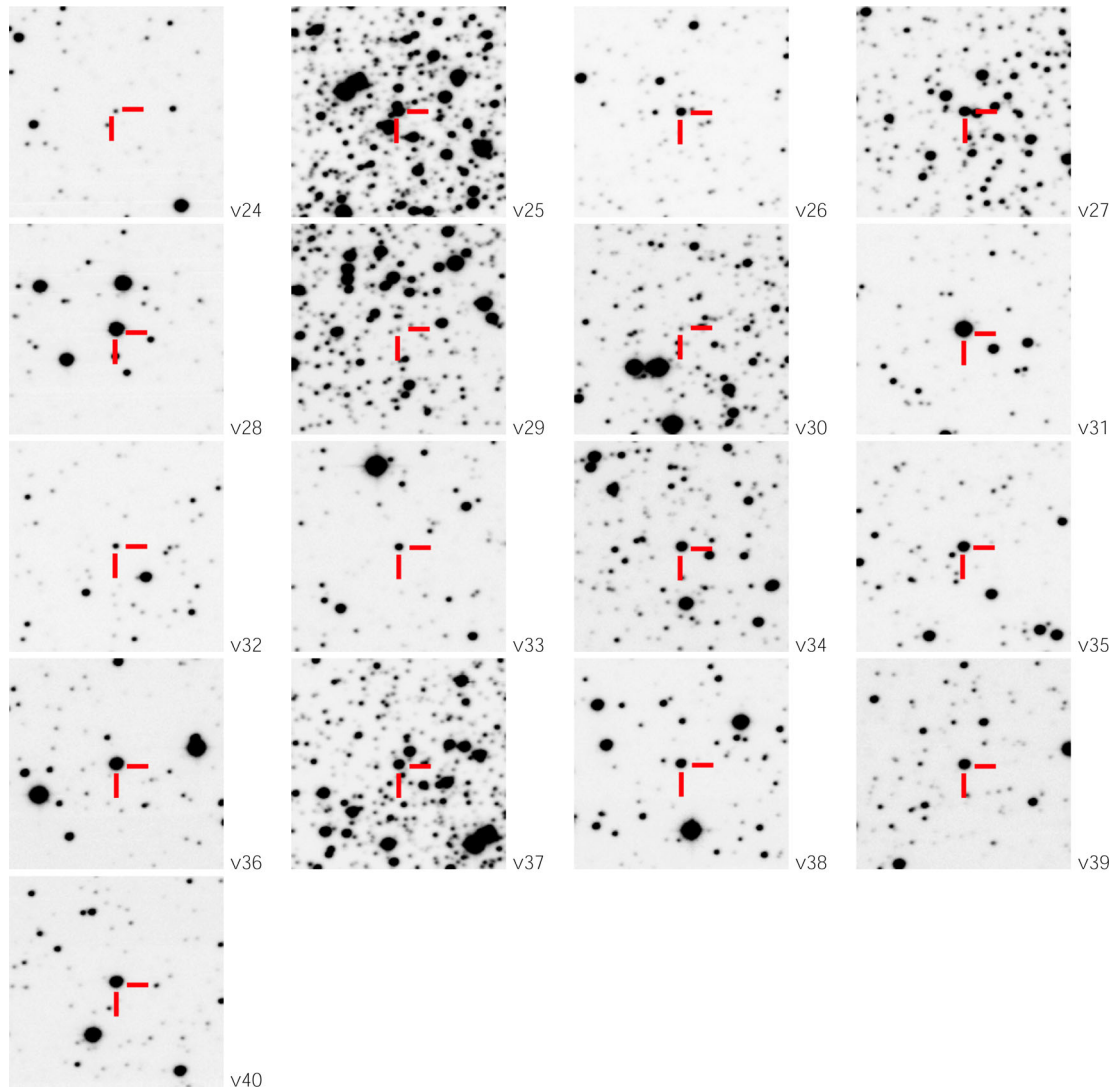
Figure 8. Finding charts for the 17 new variables (v24–v40) discovered here. The charts are each 1 arcmin × 1 arcmin and taken from the WFC *V* data described in Section 2.2. North is up and east is left.

5.4 No RRL stars in M71?

One striking thing to note about M71 is the lack of RRL variable stars discovered in previous surveys. RRL variables are old, metal-poor, Population II, pulsating horizontal branch (HB) stars and make up a significant fraction of all the variables known in GCs. M71 is an intermediate population cluster and is relatively metal rich (only M69 has a higher metallicity), which likely contributes to the lack of RRL stars. The CMD of AH71 places the HB of M71 at $V \approx 14.5$ which is well above the sensitivity limit of the NITES survey. However, the HB is relatively short and quite red so that a potential RRL progenitor in M71 may never evolve blue enough on the HB to reach the RRL instability strip.

The Quasar Equatorial Survey Team (QUEST) RRL survey (Vivas et al. 2004) found that fundamental mode (RRLab) and first overtone (RRLc) variables have mean *V*-band amplitudes and periods of 1.04 ± 0.24 and 0.536 ± 0.13 mag and 0.539 ± 0.009 and 0.335 ± 0.007 d, respectively. The unbinned data in Fig. 2 (black points) show that the NITES telescope has a typical photometric accuracy of ∼5 mmag at HB magnitudes in M71. The faintest stars

surveyed here ($V \approx 19$ mag) typically have an rms ≤ 0.1 mag. Therefore, given that the amplitude of variation of RRLab and RRLc stars is several orders of magnitude larger than our photometric performance on the HB of M71, and the high time resolution of our survey data, we conclude that the cluster is devoid of RRL stars with amplitudes $\Delta V \geq 0.1$ mag, within the field surveyed (11 arcmin × 11 arcmin ≈ $0.6r_t$). Further observations of the outer regions ($0.6r_t \leq r \leq 1r_t$) of M71 are required to determine if M71 is completely devoid of RRL variable stars.

6 ESTIMATING SPECTRAL TYPES AND MEMBERSHIP PROBABILITIES OF VARIABLE STARS TOWARDS M71

In order to constrain the spectral types of the variables observed in our survey, we obtained *BV* photometry of M71 using the WFC on the INT. GM00 present *BV* photometry of the cluster but do not cover all of the variable stars described in Sections 5.2 and 5.3. We plot the position of each variable star, as observed in our *BV*
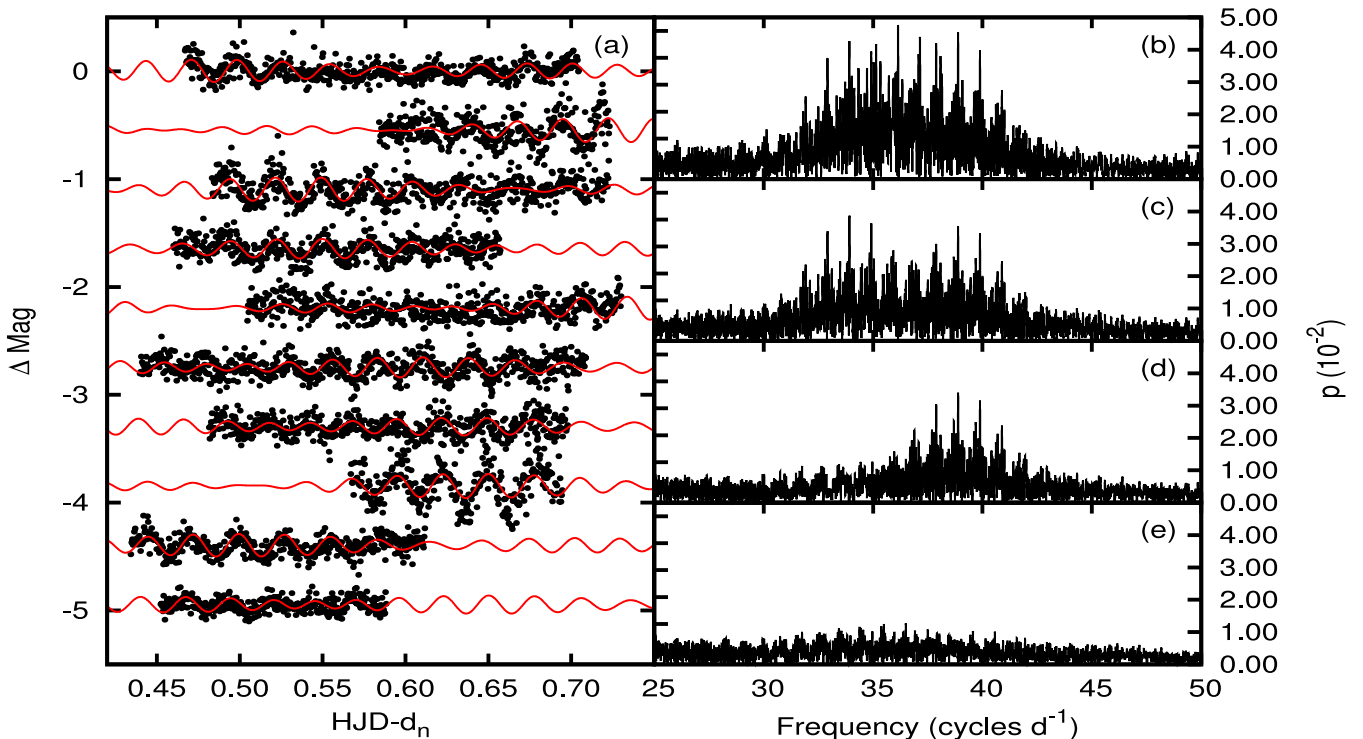
Figure 9. Light curves (left) and power spectra (right) of QU Sge. Three peaks ($f_1 = 33.9167$, $f_2 = 36.1381$ and $f_3 = 38.8864$ cycles d^{-1}) are found in the power spectrum of QU Sge out-of-eclipse data. Panel (a): Out-of-eclipse SX Phe pulsations with the best-fitting model overplotted. Beating of the frequencies detected is clearly evident on nightly inspection. The data for different nights in panel (a) have been offset by multiples of 0.55 mag for clarity; d_n is the Julian Day for a given night. Panel (b): power (p) spectrum of the raw data of QU Sge. Panel (c): power spectrum after the strongest peak ($f_2 = 36.1381$ cycles d^{-1}) has been removed. Panels (d) and (e): power spectra after the removal of the remaining two significant peaks, $f_1 = 33.9167$ cycles d^{-1} and $f_3 = 38.8864$ cycles d^{-1}, respectively.

data in Fig. 10. Stars brighter than $V = 17$ in fig. 5 of GM00 were probable cluster members as determined by their proper motion analysis. Stars fainter than $V = 17$ were taken from Hodder et al. (1992).

Janulis & Straizys (1984) measure variations in reddening towards M71 of $0.12 < E(B - V) < 0.32$. The Galactic reddening maps derived from the *IRAS* and *COBE* infrared sky surveys (Schlegel, Finkbeiner & Davis 1998)[10] also show a variation in reddening across the face of the cluster. We assume the reddening towards each variable star of Schlegel et al. (1998) as the average reddening in a 5 arcmin × 5 arcmin area surrounding each object, see Table 3. The average reddening from 14 previous surveys of M71 in several photometric systems, 10 from Janulis & Straizys (1984) and references within, and those of GM00, AH71, Cudworth (1985, hereafter CW85) and Grundahl, Stetson & Anderson (2002) gives $E(B - V) = 0.29$. The Schlegel et al. (1998) maps indicate a mean reddening of $E(B - V) = 0.305$ towards M71 (Grundahl et al. 2002), which is in agreement with the general consensus of previous studies. We calculate the intrinsic $(B - V)_0$ and V_0 for each variable star using the values of Schlegel et al. (1998), assuming $A_V/E(B - V) = 3.1$ and subsequently estimate a small range of spectral types for each variable using the transformations of Schmidt-Kaler (1982), see Table 3. As the spectral type conversions of Schmidt-Kaler (1982) require knowledge of the star's luminosity class, we quote a range of spectral types, for which the MS and giant star transformations of Schmidt-Kaler (1982) encompass the

intrinsic $(B - V)_0$ colour. Spectroscopy of the variable stars towards M71 is needed to confirm their spectral types, distances and cluster membership probabilities more rigorously.

v36 appears on Simbad as an M2.5 giant (the only variable star in M71 with a known spectral type) but with no reference to its classification. CW85 determines S4 (V4) to be a field star based on its proper motion and he calculates that QU Sge (2-255, V3) has a marginal cluster membership probability of 51 per cent. Liller & Tokarz (1981) also show QU Sge to be a non-member based on its RV but Jeon et al. (2006) argue against this. In Section 5.2, we also determine QU Sge to be a non-member based on the period–luminosity relation of the SX Phe pulsating component of the system. Of the remaining variables presented here, only three others were included in the CW85 proper motion survey of M71. v22 (KC 2-216), v34 (KC 1-91) and v37 (KC 1-38) have cluster membership probabilities of 15, 0 and 79 per cent, respectively. The additional names in parentheses given above for S4, QU Sge, v22, v34 and v37 are those of CW85.

Using the period–luminosity relation of McNamara (2011) (equation 1) and V_0, we calculate distances in parsecs to each of the δ Scuti-like variables towards M71. Assuming that the fundamental frequency has been detected, we find that all but one (v28) of the δ Scuti-like variables v26–v30 are located at large distances behind the cluster, see Table 3. v28 is the shortest period variable detected here, consistent with an SX Phe-type variability and is found to be in the foreground of the cluster at $d = 1.40 \pm 0.05$ kpc. If the period which we have identified is the first overtone rather than the fundamental, then the distances we have determined will be shorter by ~15 per cent.

[10] http://irsa.ipac.caltech.edu/applications/DUST/
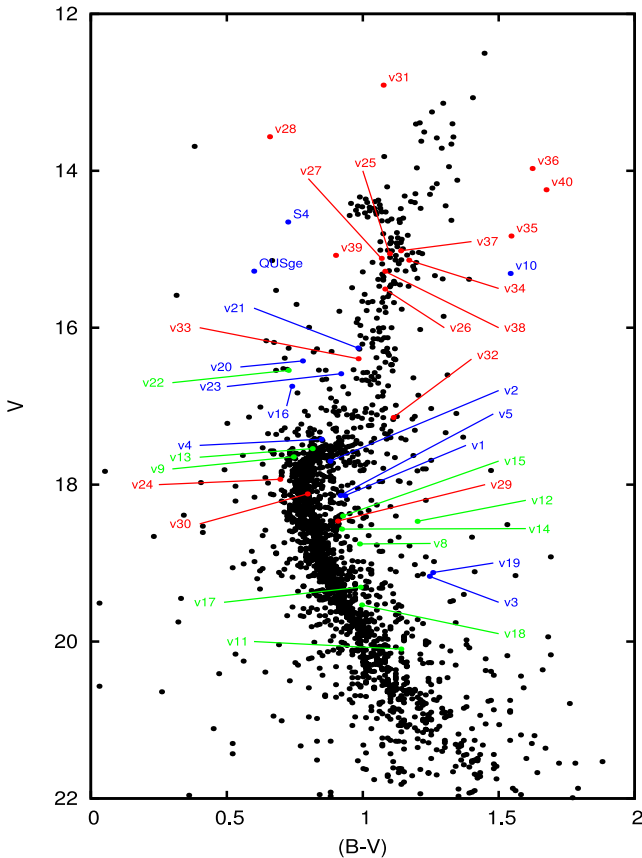
Figure 10. Fig. 4 of GM00 overplotted with the photometry of the variable star population measured from our WFC data. Stars in red denote newly discovered variable stars, those in blue show the previously known objects and those in green denote previously known objects that were not observed in the NITES survey.

Within the area surveyed, we find no evidence for RRL variables towards M71; hence, the ratios of different types of variables in M71 differ significantly from the variable star ratios in GCs of Clement et al. (2001). From the literature they estimate that ∼60 per cent of variable stars in GCs are RRL, ∼4 per cent are eclipsing binaries, 4 per cent are SX Phe variables, 2 per cent are Cepheids and 4 per cent are semi-regular variables. Based on the current population of 40 variable stars towards M71, we find that 40 per cent are eclipsing binaries, 5 per cent are δ Sct like, 2.5 per cent semi-regular and 8 per cent are long or multiply periodic variables of undefined type.

7 SUMMARY

Our high-cadence observations of M71 have revealed an additional 17 previously undiscovered variable stars towards the cluster, one of which is a detached eclipsing binary, two are possible eclipsing binary systems, five are δ Scuti-like variables, five are long-period variable stars of an as yet undefined type and three are possible semi-regular variables. We confirm the variability of 13 previously known variables and refine or calculate for the first time periods for seven of them. Our data show that the non-member S4 is most likely a detached eclipsing binary and not an RRL variable as previously suggested, and v16 appears to show variations of differing depths, suggesting an eclipsing binary rather than an SX Phe-type variable as proposed by PN00.

We estimate spectral types for 38 of 40 variables towards M71 (see Table 3), v6 and v7 which could not be identified with confidence in our WFC data and were subsequently excluded from our analysis. We cross-correlate our catalogue of variable stars with the proper motion survey of CW85 and find cluster membership probabilities for five variable stars (QU Sge, S4, v22, v34 and v37), three of which are non-members and two probable members. None have a high probability of belonging to M71. As M71 is located at low Galactic latitude, we expect increased contamination of variable stars from the field along the line of sight to the cluster, compared to other GCs in the halo. We estimate distances to six variable stars towards M71 (QU Sge, v26, v27, v28, 29 and v30) using the period–luminosity relation of McNamara (2011), finding that all but one lie at large distances behind the cluster, assuming that the fundamental mode of oscillation has been detected. Continued observation of M71 is also required to constrain any periodicity in six of the newly discovered variable stars for which a period could not be constrained.

Our search for giant transiting planets revealed five significant transit-like detections. However, none of these were consistent with a typical hot Jupiter signal. Two are the new short-period, low-amplitude variable stars v38 and v30, one is the probable eclipsing binary v10 of PN00 (which is confirmed here) and the light curves of the remaining two objects are inconsistent with giant transiting planet-like detections when folded on the periods detected. As only a small fraction of the MS in M71 was surveyed with the NITES telescope, it is difficult to constrain the giant planet frequency in M71 with confidence. Continued observation of a larger fraction of the MS is required to place limits on the giant planet frequency. To increase the likelihood of detecting a transiting hot Jupiter in M71, or any GC for that matter, requires deeper observations of a more significant fraction of the cluster's MS. In the case of M71, to do so would require photometry from a larger facility (1–2 m class telescopes, e.g. WFC on INT) to reach the photometric precision required to detect transiting giant planets at fainter magnitudes.

We have shown that the NITES telescope is sensitive to low-amplitude variability (<0.02 mag) and well suited to its future role as a follow-up telescope for transiting exoplanets. The recent discovery of transiting Neptune-sized planets in the old OC NGC 6811 (Meibom et al. 2013) has shown that planets do indeed survive in OCs. Hence, new surveys of younger, more metal rich OCs using the NITES telescope could discover more transiting giant exoplanets in the future.

REFERENCES

Alard C., Lupton R. H., 1998, ApJ, 503, 325
Arp H. C., Hartwick F. D. A., 1971, ApJ, 167, 499 (AH71)
Beatty T. G., Gaudi B. S., 2008, AJ, 686, 1302
Bergbusch P. A., VandenBerg D. A., 2001, ApJ, 556, 322

Bertin E., Arnouts S., 1996, A&AS, 117, 393

Bramich D. M. et al., 2005, MNRAS, 359, 1096

Breger M. et al., 1993, A&A, 271, 482

Burke C. J., Gaudi B. S., DePoy D. L., Pogge R. W., 2006, AJ, 132, 210

Clement C. M. et al., 2001, AJ, 122, 2587

Cudworth K. M., 1985, AJ, 90, 65 (CW85)

Cumming A., Marcy G. W., Butler R. P., 1999, ApJ, 526, 890

Cumming A., Butler R. P., Marcy G. W., Vogt S. S., Wright J. T., Fischer D. A., 2008, PASP, 120, 531

Dravins D., Lindegren L., Mezey E., Young A. T., 1998, PASP, 110, 610

Eastman J., Siverd R., Gaudi B. S., 2010, PASP, 122, 935

Elsner R. F. et al., 2008, ApJ, 687, 1019

Erben T. et al., 2005, Astron. Nachr., 326, 432

Geffert M., Maintz G., 2000, A&AS, 144, 227 (GM00)

Gilliland R. L. et al., 2000, ApJ, 545, L47

Goldsbury R., Richer H. B., Anderson J., Dotter A., Sarajedini A., Woodley K., 2010, AJ, 140, 1830

Gould A., Dorsher S., Gaudi B. S., Udalski A., 2006, Acta Astron., 56, 1

Graham M. J., Drake A. J., Djorgovski S. G., Mahabal A. A., Donalek C., Duan V., Maker A., 2013, MNRAS, 434, 3423

Grundahl F., Stetson P. B., Andersen M. I., 2002, A&A, 395, 481

Harris W. E., 1996, AJ, 112, 1487

Hodder P. J. C., Nemec J. M., Richer H. B., Fahlman G. G., 1992, AJ, 103, 460

Hood B. et al., 2005, MNRAS, 360, 791

Howard A. W. et al., 2012, ApJ, 201, 15

Huang R. H. H., Becker W., Edmonds P. D., Elsner R. F., Heinke C. O., Hsieh B. C., 2010, A&A, 513, A16

Janulis R., Straizys V., 1984, Ap&SS, 100, 95

Jeon Y. B., Kim S. L., Lee M. G., Lee H., Lee J. W., 2006, ApJ, 636, L129

Johnson J. A., Aller K. M., Howard A. W., Crepp J. R., 2010, PASP, 122, 894, 905

Kovács G., Zucker S., Mazeh T., 2002, A&A, 391, 369

Kuschnig R., Weiss W. W., Gruber R., Bely P. Y., Jenkner H., 1997, A&A, 328, 544

Lenz P., Breger M., 2005, Commun. Asteroseismol., 146, 53

Liller M. H., Tokarz S. P., 1981, AJ, 86, 669

Lomb N. R., 1976, Ap&SS, 39, 447

Marcy G., Butler R. P., Fischer D., Vogt S., Wright J. T., Tinney C. G., Jones H. R. A., 2005, Prog. Theor. Phys. Suppl., 158, 24

Mayor M. et al., 2011, preprint (arXiv:1109.2497)

McCormac J., Pollacco D., Skillen I., Faedi F., Todd I., Watson C. A., 2013, PASP, 125, 548

McNamara D. H., 2011, AJ, 142, 110

Meibom S., 2011, Am. Astron. Soc. Meeting Abstr. 218, 311.03

Meibom S. et al., 2013, Nature, 499, 55

Mochejska B. J. et al., 2005, AJ, 129, 2856

Mochejska B. J. et al., 2006, AJ, 131, 1090

Park N. K., Nemec J. M., 2000, AJ, 119, 1803 (PN00)

Pepper J., Stanek K. Z., Pogge R. W., Latham D. W., DePoy D. L., Siverd R., Poindexter S., Sivakoff G. R., 2008, AJ, 135, 907

Pollacco D. L. et al., 2006, PASP, 118, 1407

Poretti E. et al., 2005, A&A, 440, 1097

Press W. H., Rybicki G. B., 1989, ApJ, 338, 277

Quinn S. N. et al., 2012, ApJ, 756, L33

Roberts D. H., Lehar J., Dreher J. W., 1987, AJ, 93, 968

Sawyer H. B., 1953, J. R. Astron. Soc. Can., 47, 229

Sawyer Hogg H., 1973, Publ. David Dunlap Obs., 3, 6

Scargle J. D., 1982, ApJ, 263, 835

Schlegel D. J., Finkbeiner D. P., Davis M., 1998, ApJ, 500, 525

Schmidt-Kaler T., 1982, in Schaifers K., Voigt H.-H., eds, Landolt-Brnstein New Series, Group 6, Vol. 2b, Stars and Star Clusters. Springer, Berlin

Skottfelt J. et al., 2013, A&A, 553, A111

Smolinski J. P. et al., 2011, AJ, 141, 89

Stellingwerf R. F., 1978, ApJ, 224, 953

Stetson P. B., 1987, PASP, 99, 191

Street R. A. et al., 2003, MNRAS, 340, 1287

Vivas A. K. et al., 2004, AJ, 127, 1158

Weldrake D. T. F., Sackett P. D., Bridges T. J., Freeman K. C., 2005, ApJ, 620, 1043

Weldrake D. T. F., Sackett P. D., Bridges T. J., 2008, ApJ, 674, 1117

Wozniak P. R., 2000, Acta Astron., 50, 421

Wright J. T., Marcy G. W., Howard A. W., Johnson J. A., Morton T. D., Fischer D. A., 2012, ApJ, 753, 160

Yan L., Mateo M., 1994, AJ, 108, 1810

APPENDIX A: PHOTOMETRIC PERFORMANCE AND NOISE ANALYSIS OF THE NITES TELESCOPE

During our survey of M71 the photometric performance of the system was measured using full moon and first quarter observations and compared to a theoretical noise model. The noise model combines errors from the target, sky, read noise, dark current and scintillation with an estimation of the error in the flat-fielding process using equation (A1):

$$N_{\mathrm{total}} = \sqrt{f + f_{\mathrm{sky}} + \mathrm{DC} + (N_{\mathrm{r}})^2 + N_{\mathrm{flat}} + N_{\mathrm{sc}}^2}, \tag{A1}$$

where $f, f_{\mathrm{sky}}, \mathrm{DC}$ and N_{r} are the flux from the target, sky, dark current and the read noise inside the photometry aperture, respectively and

$$N_{\mathrm{flat}} = \frac{f \times n_{\mathrm{pix}}}{\sqrt{F_{\mathrm{total}}}} \text{ and} \tag{A2}$$

$$N_{\mathrm{sc}} = 0.09 D^{-2/3} (\sec(Z))^W \exp\left(\frac{-h}{h_0}\right) (2t)^{-1/2} \tag{A3}$$

are the errors from flat-fielding and the scintillation noise according to Dravins et al. (1998), respectively. n_{pix} is the number of pixels inside the photometric aperture, F_{total} is the combined flux in e^- pixel^{-1} in the master flat-field (typically $\sim 1\,000\,000$ e^- pixel^{-1}), D is the diameter of the telescope aperture in cm, $\sec(Z)$ is the airmass, h is the altitude of the observatory in m, $h_0 = 8000$ m is the atmospheric scaleheight, t is the integration time in s and W is a variable dependent on angle between the line of sight and wind direction. $W = 1.5, 1.75$ or 2.0 when observing perpendicular to the wind, close to the zenith and parallel to the wind, respectively.

The image-subtracted frames (see Section 2.1) typically have a background level with a mean flux ≈ 0; hence, measuring the sky level directly is impossible. However, the noise from the sky will remain in the subtracted images and is expected to be Gaussian in nature. Hence, by measuring the standard deviation in the background of each subtracted image, the flux from the sky in the photometry aperture f_{sky} in e^- can be estimated using

$$f_{\mathrm{sky}} = \sigma_{\mathrm{sky}}^2 \times G \times n_{\mathrm{pix}}, \tag{A4}$$

where σ_{sky} is the nightly average standard deviation of the background in the subtracted images and G is the gain in e^- ADU^{-1}.

Fig. A1 (left and centre) shows the noise model of the NITES telescope along with the typical photometric accuracy during dark and bright time, respectively. It is evident from Fig. A1 (right) that the noise in the system is essentially Gaussian as the data points follow the $\sqrt{n}$ decrease in rms, where n is the number of binned points. Fig. A1 (right) demonstrates that the system is relatively free from systematic noise down to the sub-mmag regime. A photometric accuracy of 1 mmag is reached with binned exposure times of ≈ 400 s during dark time while bright time observations reach rms < 2 mmag on the same time-scale.
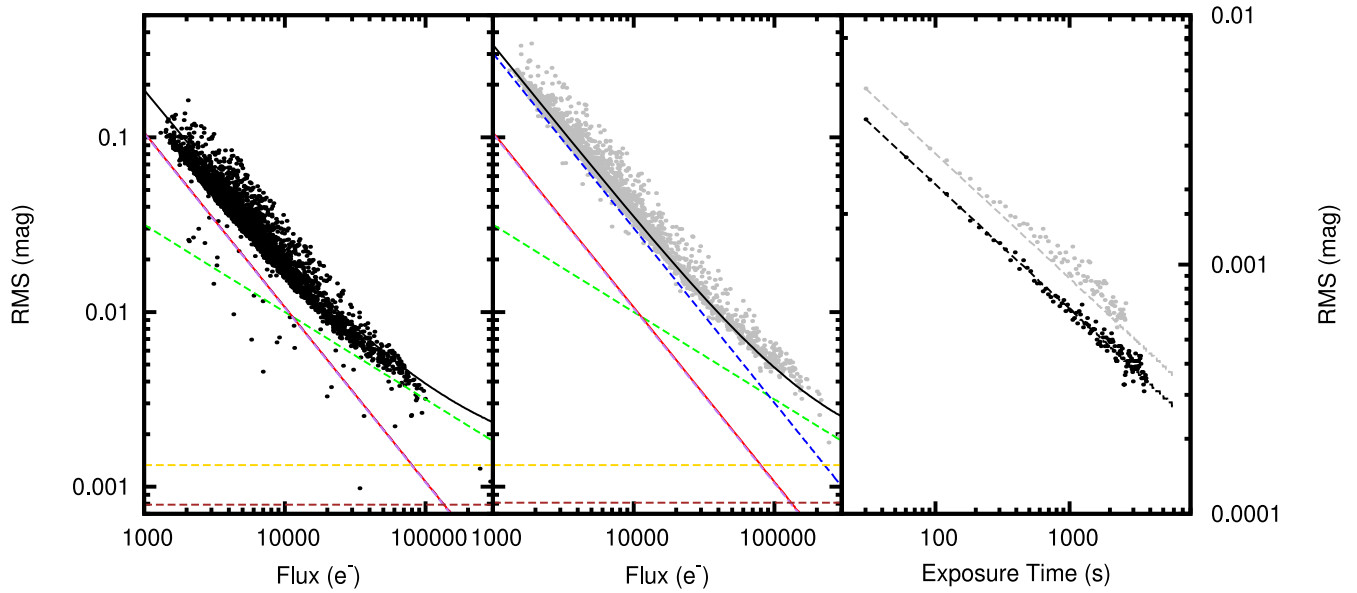
Figure A1. Black and grey points represent data taken during dark and bright time, respectively. The left and middle plots are rms versus flux diagrams taken during dark and bright time, respectively. The right plot shows the rms versus binned exposure time for the average of the nine brightest non-variable stars during bright and dark time. The green, blue, red, purple, yellow and brown dashed lines represent the noise models from the target, sky, read noise, dark current, scintillation and flat-fields, respectively. In the left-hand panel, the noise models of the sky, dark current and read noise (blue, purple and red dashed lines) are almost completely overlapping. In the central panel, the noise models of the dark current and read noise (purple and red dashed lines) are also overlapping. The solid black line represents the total noise model, while the black and grey dashed lines show the expected $\sqrt{n}$ decrease in rms in the presence of Gaussian noise only, where n is the number of points per bin.

This paper has been typeset from a TeX/LaTeX file prepared by the author.